



Acute tear versus chronic-degenerated rotator cuff pathologies are associated with divergent tendon metabolite profiles

Katie J. Sikes ^a, Kendra M. Andrie ^{b,c}, Sara Wist^a, Nikhil Verma^d, Adam B. Yanke ^d, Kelly S. Santangelo ^b, David D. Frisbie^a, and Brian J. Cole ^d

^aDepartment of Clinical Sciences, Colorado State University, Fort Collins, USA; ^bDepartment of Microbiology, Immunology, and Pathology, Colorado State University, Fort Collins, USA; ^cIDEXX Laboratories, Inc, Westbrook, ME, USA; ^dDepartment of Orthopaedic Surgery, Rush University Medical Center, Chicago, USA

ABSTRACT

Purpose/Aim: Metabolic disorders are risk factors for rotator cuff injuries, which suggests that the rotator cuff is sensitive to local metabolic fluctuations. However, the link between the metabolic microenvironment and pathologic features of acute tear versus chronic degeneration is currently unknown. The overarching goal of this study was to evaluate alterations in tendon metabolite profiles following acute tear or chronic degeneration of the rotator cuff. We hypothesized that injury types (acute tear vs. chronic degeneration) would result in distinct metabolite profiles relative to clinically unaffected tendon controls.

Materials and Methods: We utilized untargeted metabolomics to identify pathways that were altered at the time of rotator cuff repair (RCR; acute tear) or reverse total shoulder arthroplasty (rTSA; chronic degeneration) relative to total shoulder arthroplasty controls (TSA; tendon clinically unaffected).

Results: Acute tears to the rotator cuff were associated with an overall decrease in tendon metabolites. This global decrease was primarily associated with glycolic acid and decreased tricarboxylic acid (TCA) cycle activity. Conversely, chronic tendon specimens from patients undergoing rTSA showed an overall increase in metabolites. Most notably, chronic injury was associated with increased levels of multiple amino acids including alanine, aspartate, lysine, and proline.

Conclusions: Overall, this study demonstrates that distinct metabolite profiles are associated with injury types, and that therapeutic strategies should address both cellular and matrix components regardless of injury induction. The specific pathways identified paired with validated, established, treatment methods may serve as novel therapeutic targets for patients who suffer from rotator cuff injuries.

ARTICLE HISTORY

Received 10 October 2023

Revised 18 October 2024

Accepted 13 May 2024

KEYWORDS

Rotator Cuff Tendon;
Metabolomics; Metabolism;
Rotator Cuff Repair; Reverse
Total Shoulder Arthroplasty

Introduction

Numerous metabolic disorders, including increased fasting glucose¹ and diabetes,^{2,3} hypercholesterolemia,⁴ and hyperuricemia,⁵ have been identified as risk factors for rotator cuff injuries. This link between systemic metabolic dysfunction and rotator cuff pathologies suggests that the rotator cuff is sensitive to metabolic shifts and that local metabolic fluctuations may be associated with injury. However, the extent to which metabolic changes within the rotator cuff tendon are linked to pathologic features following either acute tear or chronic degeneration is currently unknown.

Repetitive overuse of the rotator cuff tendon induces microdamage within the highly organized extracellular matrix,⁶ which, if not balanced with rest, initiates cellular cascades responsible for chondroid metaplasia, fatty

infiltration, and collagen disorganization, all hallmarks of chronic tendon degeneration or tendinopathy.^{7–11} In contrast, acute tears of the rotator cuff, due to trauma, are characterized by a defined macroscopic loss of tendon continuity (either partial or full thickness), followed by formation of a fibrotic scar¹² associated with collagen synthesis dysregulation.¹³ Both etiologies result in loss of mechanical function and pain and require surgical intervention either with a reverse total shoulder arthroplasty for chronic degeneration or rotator cuff repair for an acute tear. While these techniques primarily seek to restore mechanical function, they do not address the underlying cellular metabolic changes that may contribute to the high prevalence of revision surgeries associated with rotator cuff injuries. As a first step in addressing this gap, there is a critical need to understand

CONTACT Katie J. Sikes  Katie.Sikes@colostate.edu  Department of Clinical Sciences, Colorado State University, 1621 Campus Delivery, Fort Collins, CO 80523-1621, USA

 Supplemental data for this article can be accessed online at <https://doi.org/10.1080/03008207.2024.2425867>

© 2024 Informa UK Limited, trading as Taylor & Francis Group

the relationship between tendon metabolism and injury,¹⁴ particularly in the rotator cuff.

A recent metabolomics study focusing on shoulder stiffness due to impingement syndrome or lesions in the long head of the biceps found lipid-related metabolite changes in the rotator interval and anterior capsule, specifically associated with sphingomyelin glycerophospholipids.¹⁵ Additionally, high correlations in these altered metabolites were associated with serum cholesterol, which may be associated with shoulder stiffness.¹⁵ While informative to other shoulder pathologies, this study excluded patients with pathology to the rotator cuff tendons. Furthermore, rotator cuff studies have primarily focused on muscle, as opposed to tendon, related metabolic changes. In patients with rotator cuff tears, 2-[(18F)-fluoro-2-deoxy-d-glucose (FDG) uptake measured via positron emission tomography (PET) was decreased in the supraspinatus and infraspinatus muscles relative to the contralateral non-injured muscles.¹⁶ Notably, by 6 months following surgical repair, glucose uptake in the supraspinatus muscle was no longer significantly different from the non-injured side.¹⁷ To date, no studies have analyzed rotator cuff tendon clinical specimens for altered metabolite changes.

The overarching goal of this study was to evaluate alterations to tendon metabolite profiles following acute tear or chronic degeneration of the rotator cuff. We hypothesized that injury type (e.g., acute tear vs. chronic degeneration) would result in distinct metabolite profile differences relative to clinically unaffected tendon controls. To test this, we utilized untargeted metabolomics to identify metabolic pathways that were altered at the time of rotator cuff repair (RCR; acute tear) or reverse total shoulder arthroplasty (rTSA; chronic degeneration) relative to total shoulder arthroplasty controls (TSA; tendon clinically unaffected). Understanding the relationship between injury and cellular metabolism in the rotator cuff may allow for the identification of novel strategies for the treatment of both acute tear and chronic degeneration rotator cuff pathologies.

Methods

Specimen collection

Under IRB approval and with patient consent (Rush University Medical Center; #17011032), tendon specimens were taken at the time of Rotator Cuff Repair (RCR, acute tear injury, $n = 14$, for metabolomics only), Reverse Total Shoulder Arthroplasty (rTSA, chronic degeneration, $n = 15$, each specimen analyzed for both

metabolomics and histology), and Total Shoulder Arthroplasty (TSA, clinically unaffected tendon, separate $n = 16$ for metabolomics and $n = 14$ for histology). Due to size limitations during specimen retrieval, all specimens were not able to be used for all analyses. Specified donor age was between 40 and 85 years of age, with exclusion criteria for the history of radiation of upper extremities and tobacco use. Only patients who had failed appropriate non-surgical management for at least 6 months qualified. For each specimen, the following clinical parameters were noted: 1) age, 2) sex, 3) duration of symptoms, 4) time between diagnosis and surgery, 5) prior non-surgical failed treatments such as injections or physical therapy, and 6) diabetes. Specimens collected for metabolomics were immediately (within 10 min of retrieval) frozen in liquid nitrogen and stored at -80°C until analysis. Specimens collected for histology were placed into 10% neutral buffered formalin until analysis.¹⁸

Histology and histopathology

Following fixation in 10% neutral buffered formalin, rTSA and TSA specimens were processed, embedded in paraffin, and $5\mu\text{m}$ longitudinal sections were obtained. Sections were deparaffinized and stained with Hematoxylin and Eosin (H&E). Slides were graded by a Board-Certified Veterinary Pathologist for both the Bonar¹⁹ and Movin²⁰ Tendinopathic Scoring Guidelines following standards established within the field.¹⁸ All slides were blinded prior to grading, and all groups were analyzed together within the same timeframe.

Metabolomic specimen processing

Tissue samples were pulverized in a chilled mortar and pestle, weighed (for normalization of raw metabolite abundances to specimen weight), placed in 1 mL of 50% methanol, and transferred to the Analytical Resources Core—Bioanalysis and Omics (ARC-BIO) at Colorado State University for metabolomics processing. For specimens submitted to metabolomics, the average (average (STD)) weight for each group was as follows: RCR 225.72 mg (138.28 mg), rTSA 294.82 mg (90.85), TSA 267.41 mg (96.52 mg). Using a QsonicaTM sonicator, the samples were sonicated 10 s on and 20 s off for 30 min at an amplitude of 80%. The supernatant was transferred to a new vial and evaporated under nitrogen. To ensure appropriate tissue fragmentation, two additional sonication steps were completed. First, sonication was conducted using 1 mL of 100% ULCMS-grade methanol for 15 min with the

previous settings. The resultant extract was then completely evaporated under nitrogen and stored at $-20\text{ }^{\circ}\text{C}$. Second, sonification was conducted using 500 μL MTBE and 500 μL 75% MeOH/25% water for 30 min in a cold-water bath, then shaking for 2.5 h at $4\text{ }^{\circ}\text{C}$ before further sonification for 30 min in a cold-water bath. Samples were then centrifuged for 15 min at 3500 rpm at $4\text{ }^{\circ}\text{C}$ and the supernatant was added to the same vial holding previous sample extracts and completely evaporated under nitrogen.

This pooled extract was then divided into two separate fractions by using a biphasic procedure. 1 mL of cold MTBE:MeOH:Water (6:3:1) was added to the vial, followed by 350 μL water. Samples were vortexed for 20 min at $4\text{ }^{\circ}\text{C}$ to ensure resuspension. The biphasic system was centrifuged for 15 min at 3500 rpm at $4\text{ }^{\circ}\text{C}$. A 400 μL aliquot of the organic layer was completely evaporated under nitrogen and resuspended in 160 μL of UPLCMS-grade 1:1 toluene/methanol and the upper and lower layers transferred to separate vials for further processing. The remaining organic layer was washed with 100% MTBE and completely removed from the remaining aqueous layer. The aqueous layer was diluted with 900 μL of 2:2:1 acetonitrile/methanol/water and incubated for 1 h at $-80\text{ }^{\circ}\text{C}$ and then for 1 h at $-20\text{ }^{\circ}\text{C}$. The samples were centrifuged for 15 min at 3750 rpm and $4\text{ }^{\circ}\text{C}$, and the cold incubation and centrifugation were repeated. 1 mL of the supernatant was transferred to a new 2 mL clear glass autosampler and then diluted a second time with 500 μL of 2:2:1 acetonitrile/methanol/water and briefly vortexed. The samples were incubated overnight at $-20\text{ }^{\circ}\text{C}$ prior to centrifuging for 15 min at 3750 rpm and $4\text{ }^{\circ}\text{C}$. 600 μL of supernatant was transferred to a clean 2 mL glass vial, which was then completely evaporated under nitrogen and re-suspended in 300 μL of 2:2:1 acetonitrile/methanol/water and briefly vortexed. After an overnight incubation at $-20\text{ }^{\circ}\text{C}$, the samples were centrifuged for 15 min at 3750 rpm and $4\text{ }^{\circ}\text{C}$. 200 μL of supernatant was transferred to a new 2 mL clear glass autosampler vial for GC-MS analysis. ULCMS grade water was utilized for all extraction steps.

Gas chromatography Mass spectroscopy (GCMS; polar metabolomics)

The aqueous phase re-suspension was dried under nitrogen, re-suspended in 30 μL of pyridine containing 25 mg/mL of methoxyamine hydrochloride, incubated at $60\text{ }^{\circ}\text{C}$ for 1 h, sonicated for 10 min, and incubated for an additional 1 h at $60\text{ }^{\circ}\text{C}$. Next, 30 μL of N-methyl-N-trimethylsilyltrifluoroacetamide with 1% trimethylchlorosilane (MSTFA +1% TMCS, Thermo Scientific) was added, and samples were incubated at $60\text{ }^{\circ}\text{C}$ for

45 min, briefly centrifuged, cooled to room temperature, and 100 μL of the supernatant was transferred to a 150 μL glass insert in a GC-MS autosampler vial. Metabolites were detected using a Trace 1310 GC coupled to a Thermo ISQ mass spectrometer (Thermo Scientific). Samples were injected in a 1:10 split ratio. Separation occurred using a 30 m TG-5 MS column (Thermo Scientific, 0.25 mm i.d., 0.25 μm film thickness) with a 1.2 mL/min helium gas flow rate, and the program consisted of $80\text{ }^{\circ}\text{C}$ for 30 sec, a ramp of $15\text{ }^{\circ}\text{C}$ per min to $330\text{ }^{\circ}\text{C}$, and an 8 min hold. Masses between 50 and 650 m/z were scanned at 5 scans/sec after electron impact ionization.

Ultra-high performance liquid chromatography Mass spectroscopy (UPLCMS; non-polar metabolomics)

Aliquots of different volumes of the organic layer from sample extraction (normalized according to sample weight) were taken and suspended in 400 μL of 1:1 toluene methanol to normalize for weight variations between the original sample tissues. Samples were diluted 20-fold with 1:1 toluene/methanol prior to injecting 1 μL of extract onto a Waters Acquity UPLC system in randomized order. Separation was achieved using a Waters Acquity UPLC CSH Phenyl Hexyl column (1.7 μm , $1.0 \times 100\text{ mm}$), using a gradient from solvent A (Water, 0.1% ammonium formate) to solvent B (Acetonitrile, 0.1% formic acid). Injections were made at 99% A, held at 99% A for 1 min, ramped to 98% B over 12 min, held at 98% B for 3 min, and then returned to starting conditions over 0.05 min and allowed to re-equilibrate for 3.95 min, with a 200 $\mu\text{L}/\text{min}$ constant flow rate. The column and samples were held at $65\text{ }^{\circ}\text{C}$ and $6\text{ }^{\circ}\text{C}$, respectively. The column eluent was infused into a Waters Xevo G2 Q-TOF-MS with an electrospray source in positive mode, scanning 50–2000 m/z at 0.2 s per scan, alternating between MS (6 V collision energy) and MSE mode (15–30 V ramp). Calibration was performed using sodium iodide with 1 ppm mass accuracy. The capillary voltage was held at 2200 V, source temperature at $150\text{ }^{\circ}\text{C}$, and nitrogen desolvation temperature at $350\text{ }^{\circ}\text{C}$ with a flow rate of 800 L/hr.

Data processing

Raw mass spectrometry data were processed using an R-based workflow for feature detection, retention time alignment, feature grouping, peak filling, feature clustering. XCMS (v.3.8.1) was used for feature detection and retention time alignment. Processing was performed using R (v.R Core Team 2019). Feature data

were input as an *xcms* object with *ramclustR* parameter settings of $st = 1.22$ $sr = 0.5$ and $maxt = 24.4$. *RAMClustR* for GCMS and $st = 2.7$ $sr = 0.5$ and $maxt = 54$. *RAMClustR* for UPLCMS (version 1.0.9) was utilized to cluster features into spectra.²¹ Feature data included both MS and indiscriminate MS/MS data.²² Features were normalized to total signal using “*tic*” normalization. The feature similarity matrix was clustered using *fastcluster* package hierarchical clustering method using the average method. The dendrogram was cut using the *cutreeDynamicTree* function from the *dynamicTreeCut* package. Cutting parameters were set to $minModuleSize = 2$, $hmax = 0.5$, and $deepSplit = FALSE$.

For GCMS 10,074 features were collapsed into 883 spectra. For UPLCMS, 5284 features were collapsed into 696 spectra. Molecular weight was inferred using the *do.findmain* function, which calls the *interpretMSSpectrum* package.²³ Annotations were assigned using the *RAMClustR* *annotate* function. Annotation priority was assigned from highest priority to lowest: *RAMsearch* for GMCS, and *MSFinder* spectrum search, *MSFinder* structure, *MSFinder* formula, *interpretMSSpectrum* M. *MSFinder* structures were considered from databases for UPLCMS. For GCMS, smiles structures were retrieved for each *inchikey* without a structure using the Pubchem API²⁴ called from *RAMClustR* using the *getSmilesInchi* function. Compounds were assigned to chemical ontogenies using the *ClassyFire* API.²⁴ For UPLCMS, database priority was set to HMDB SMPDB ChEBI LipidMAPS Serum Csf BLEX. Smiles structures were retrieved for each *inchikey* without a structure using the Pubchem API²⁴ called from *RAMClustR* using the *getSmilesInchi* function. Compounds were assigned to chemical ontogenies using the *ClassyFire* API.²⁴

All annotated metabolites were matched to a HMDB identification number for relevance by cross-referencing the compound name against the GOLM metabolome database.²⁵ For GCMS, 212 unique metabolites were identified from 883 spectra. For UPLCMS, 121 unique metabolites were identified from 696 spectra. GCMS and UPLCMS identified metabolites can be seen in Supplemental 1 and Supplemental 2, respectively. Chemometric analysis using partial least square discriminant analysis (PLS-DA) and pathway analysis was performed in *MetaboAnalyst* 4.0.²⁶ Chemometric analysis allowed for global data visualization through principal component plots, heatmap clustering, and variable importance in the projection (VIP). For *MetaboAnalyst*, sample abundances were not normalized (as raw metabolite abundances were previously normalized to specimen weight) or transformed but

were auto-scaled (mean-centered and divided by the standard deviation of each variable). Both GCMS and UPLCMS significant metabolites were uploaded for pathway analysis. For RCR (acute tear injury) and rTSA (chronic injury) comparisons relative to TSA controls, 115 and 15 metabolites, respectively, were identified in *MetaboAnalyst* and utilized for pathway analysis.

Statistical Analysis

All statistics were conducted in *GraphPad Prism* v10.1.2 (San Diego, CA). For patient demographic information, groups (RCR, rTSA, and TSA) were compared using a One-Way ANOVA with Tukey's Post-Hoc Comparisons. For GCMS and UPLCMS individual metabolite comparisons, groups (RCR, rTSA, and TSA) were compared using a Kruskal–Wallis test with Dunn's Post-Hoc Comparisons. For histological grading, groups (rTSA, TSA) were compared using a Mann–Whitney test. For metabolomic and histological associations for rTSA specimens, a non-parametric Spearman Correlation was conducted, with false-discovery rate (FDR) corrections conducted using a two-stage linear step-up procedure of Benjamini, Krieger, and Yekutieli with a 1% FDR. Significance for all comparisons was set to $p < 0.05$.

Results

Specimen demographics

A summary of patient demographic information can be seen in Table 1. When comparing the age of patients for each specimen group, rTSA specimens were obtained from patients of a significantly increased age relative to RCR and TSA (histology) patients ($p < 0.0001$ and $p = 0.03$, respectively). No significant differences in duration of symptoms (months) and time from diagnosis (months) were seen between groups ($p = 0.10$ and $p = 0.40$, respectively). For sex, the majority of rTSA specimens were from female patients, while the majority of TSA specimens were from male patients. When reported, diabetes was only present in at most one patient per group; therefore, due to the limited sample size, analysis of diabetes as a co-morbidity for tendon injury could not be conducted in the current study.

Histopathology

Histology was conducted on specimens obtained from rTSA (chronic tendon injury) and TSA (clinically

Table 1. Patient demographic information.

	RCR	rTSA	TSA		p-value
			Metabolomics	Histology	
Age (years)	57.85 (10.15) ^A	72.15 (5.16) ^{A,B}	64.85 (5.34)	64.33 (11.01) ^B	p = 0.0002
Duration of Symptoms (months)	58.71 (82.80)	20.67 (11.36)	164.25 (215.46)	218.4 (226.4)	p = 0.10
Time from Diagnosis (months)	11.63 (18.28)	3.5 (2.18)	2.33 (1.04)	4.8 (3.46)	p = 0.40
Sex	N = 7 F N = 7 M	N = 9 F N = 6 M	N = 4 F N = 11 M	N = 4 F N = 10 M	N/A
Diabetes	N = 1 Yes N = 5 No N = 8 NS	N = 1 Yes N = 2 No N = 12 NS	N = 15 NS	N = 0 Yes N = 2 No N = 12 NS	N/A

*Data represented as Average (Standard Deviation); One-way ANOVA p-value listed with matching superscripts denoting significant differences between groups for post-hoc comparisons; Abbreviations: F = Female, M = Male, NS = Not Specified.

unaffected tendon) patients to determine the specific degree of tendon pathology. Due to the size (approximately 1 cm³) of tissue removed during RCR (acute tear injury), histology was not possible as tissue collected was prioritized for metabolomics. TSA specimens exhibited mild collagen disruption (Figure 1(a)), slightly increased vascular profiles (Figure 1(b)), and

increased tenocytes and extracellular matrix (Figure 1(c)). rTSA specimens exhibited disruption of the collagen fibers (Figure 1(d)), with the presence of medium-to-large vacuolated lakes (Figure 1(e)) and hyalinized collagen and increased extracellular matrix (Figure 1(f)). Histopathological grading demonstrated that, relative to TSA specimens, rTSA specimens

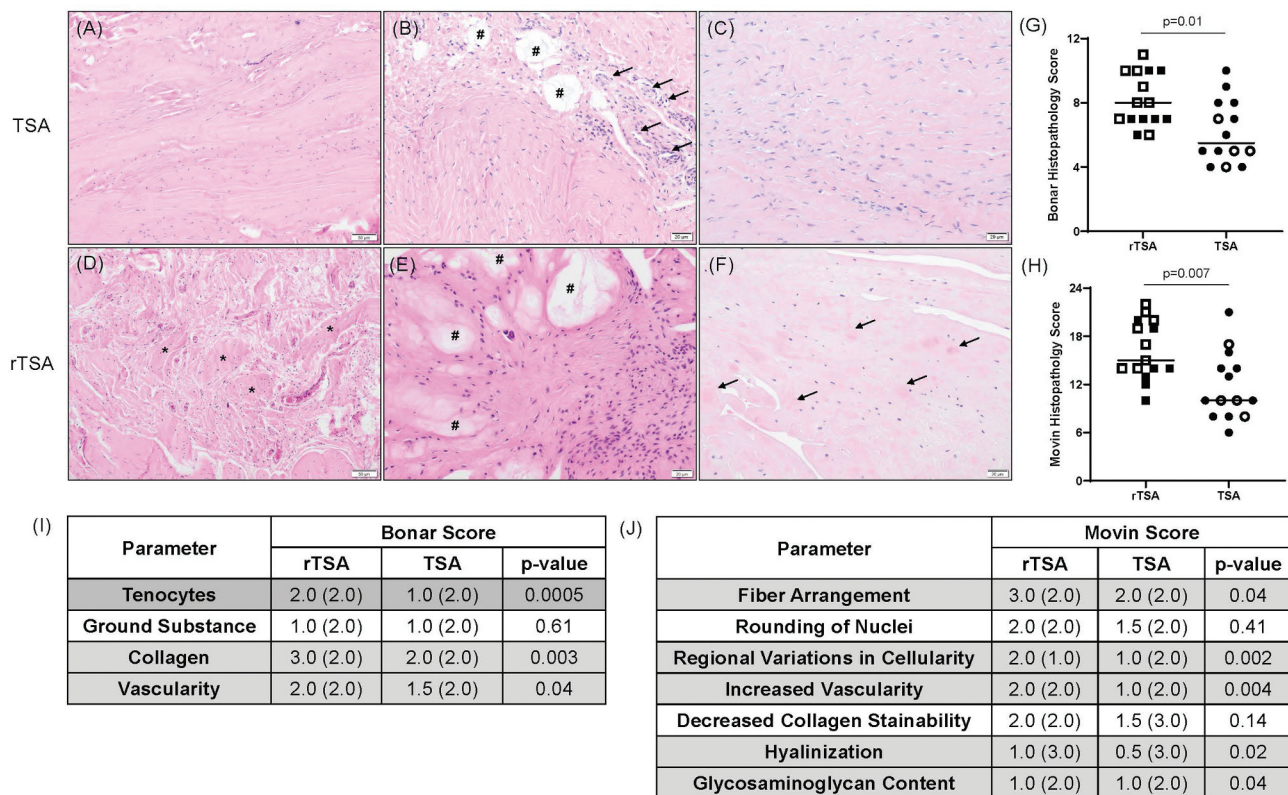


Figure 1. Representative photomicrographs of TSA (A-C) and rTSA (D-F) specimens. (A) Fiber bundles mildly undulated, with patches of slight pallor. (B) Increased vascular profiles (arrows) admixed with small to medium sized vacuolated lakes (#) containing basophilic stippled extracellular matrix. (C) Increased numbers of tenocytes and extracellular matrix between fibers. (D) Parallel arrangement of tendon fibers disrupted and dissected by haphazardly arranged collagen bundles and vascular profiles. Remnant tendon fibers highlighted with asterisk. (E) Disruption of fiber structure and arrangement due to expansion by medium to large vacuolated lakes (#) containing degenerate collagen and matrix and increased numbers of disorganized tenocytes. (F) Complete loss of fiber structure and arrangement, and replacement with hyalinized collagen (arrows) and increased amount of extracellular matrix. (G) Bonar and (H) Movin histopathology scores for TSA and rTSA specimens. Data presented as median with individual data points marked and p-values denoted. Open symbols represent specimens from female patients and closed specimens represent specimens from male patients. Individual (I) Bonar and (J) Movin parameters presented as median (range) with p-values between TSA and rTSA groups.

exhibited both a higher Bonar ($p = 0.01$; **Figure 1(g)**) and Movin score ($p = 0.007$; **Figure 1(h)**) suggestive of increased tendon pathologies. Within Bonar scoring, significant differences between groups were observed for tenocytes ($p = 0.0005$), collagen ($p = 0.003$), and vascularity ($p = 0.04$), but not ground substance ($p = 0.61$) (**Figure 1(i)**). With Movin scoring, significant differences between groups were observed for fiber arrangement ($p = 0.04$), regional variation in cellularity ($p = 0.002$), increased vascularity ($p = 0.004$), hyalinization ($p = 0.02$), and glycosaminoglycan content ($p = 0.04$), but not rounding of nuclei ($p = 0.41$) and decreased collagen stainability ($p = 0.14$) (**Figure 1(j)**). Overall, these data demonstrate that TSA specimens only displayed anticipated mild age-related degenerative background pathology relative to rTSA specimens. Notably, no sex-specific separation in Bonar or Movin scoring within the groups was appreciated (**Figure 1(g-h)**, open vs. closed symbols). Overall, the histopathologic changes observed validate that the TSA specimens can serve as an appropriate control for the metabolomic comparisons conducted in this study.

Global metabolite profiling

Based on PLS-DA analysis, no appreciable global differences in GMCS polar or UPLCMS nonpolar metabolite profiles were detected when specimens were stratified by age (Supplemental 3), duration of symptoms (Supplemental 4), and time from diagnosis (Supplemental 5), irrespective of specimen type. This was appreciated through principal component plots with overlapping groups and Variable Importance in the Projection (VIP) scores for individual metabolites all less than 2.0 or VIP scores of greater than 2.0 associated with non-consistent trends (e.g., increasing metabolite abundances not directly related to increasing duration of symptoms or time from diagnosis). Overall, this suggests that these parameters (age, duration of symptoms, and time from diagnosis) did not contribute to appreciable or clinically relevant metabolite variability in our particular sample set. When stratified by sex, irrespective of specimen type, global separation of GMCS polar metabolites was appreciated between males and females based on the principal component plot, with males generally exhibiting lower abundance of amino acids including lysine, proline, and alanine based on VIP scores of less than 2.0 (Supplemental 6). Further, the following UPLCMS nonpolar metabolites showed VIP scores of greater than 2.0 when stratified by sex with males having a lower abundance: two phosphatidylserines, one phosphatidylinositol, one diacylglycerol, one

lysophosphatidylcholine, one ceramide (*N*-docosanoyl-(4E,14Z)-sphinga-4,14-dienine), and a triterpene saponin (Tragopogonsaponin B). Due to the disparity in sample size between sexes of the different groups, individual metabolite statistical comparisons between sexes were unable to be conducted. When possible, sexes were delineated in the results to identify trends.

When separated by specimen type (RCR, rTSA, vs. TSA), the first two principal components for PLS-DA contributed to more than 40% of the separation for all comparisons (**Figure 2(a,b)**), with the remaining principal components each associated with less than 5% for GCMS and 17% for LCMS. When PLS-DA plots were paired with heatmap clustering analysis, results show that acute RCR specimens demonstrated a distinct metabolite profile relative to both normal TSA and chronic degenerated rTSA specimens. This was evident primarily for polar GCMS analysis (**Figure 2(a,c)**), with minor separation observed for nonpolar UPLCMS analysis (**Figure 2(b,d)**). While rTSA specimens were more similar to TSA specimens, some separation was evident. Individual metabolites driving variability are described below based on injury-type comparisons (e.g., acute tear vs. chronic degeneration).

Rotator cuff repair (acute tear injury) metabolomics

Relative to TSA control specimens, RCR specimens taken at the time of surgery exhibited an overall decrease in 78 polar GCMS (**Figure 3(a)**) and 43 nonpolar UPLCMS metabolites (**Figure 3(b)**), with few metabolites being significantly increased relative to controls. With respect to VIP scoring, glycolic acid was the only metabolic reaching a VIP score of greater than 2.0 (**Figure 3(c)**) denoting that glycolic acid may be a major driver of GCMS global profiling differences (**Figure 3(c)**). No metabolites reached a VIP score of greater than 2.0 for UPLCMS analyses (**Figure 3(d)**). To explore glycolic acid changes further, individual statistical analysis demonstrated that glycolic acid was significantly decreased in RCR specimens relative to TSA specimens (RCR average (STD) relative abundance 3.06×10^7 (8.37×10^7); TSA average (STD) relative abundance 8.43×10^6 (2.37×10^7); $p < 0.0001$, Supplemental 1). Despite the significance of glycolic acid itself, this metabolite did not contribute to specific pathway differences seen via pathway analysis.

Combined GMCS and UPLCMS pathway analysis revealed that five pathways associated with the citrate cycle (Tricarboxylic Acid Cycle; TCA cycle) (**Figure 3(e)**) demonstrated a Holm adjusted p -value of less than 0.05 denoting significance. Specifically, these included pyruvate metabolism (the primary source of Acetyl CoA which initiates the TCA cycle), the TCA cycle itself, and pathways associated with TCA

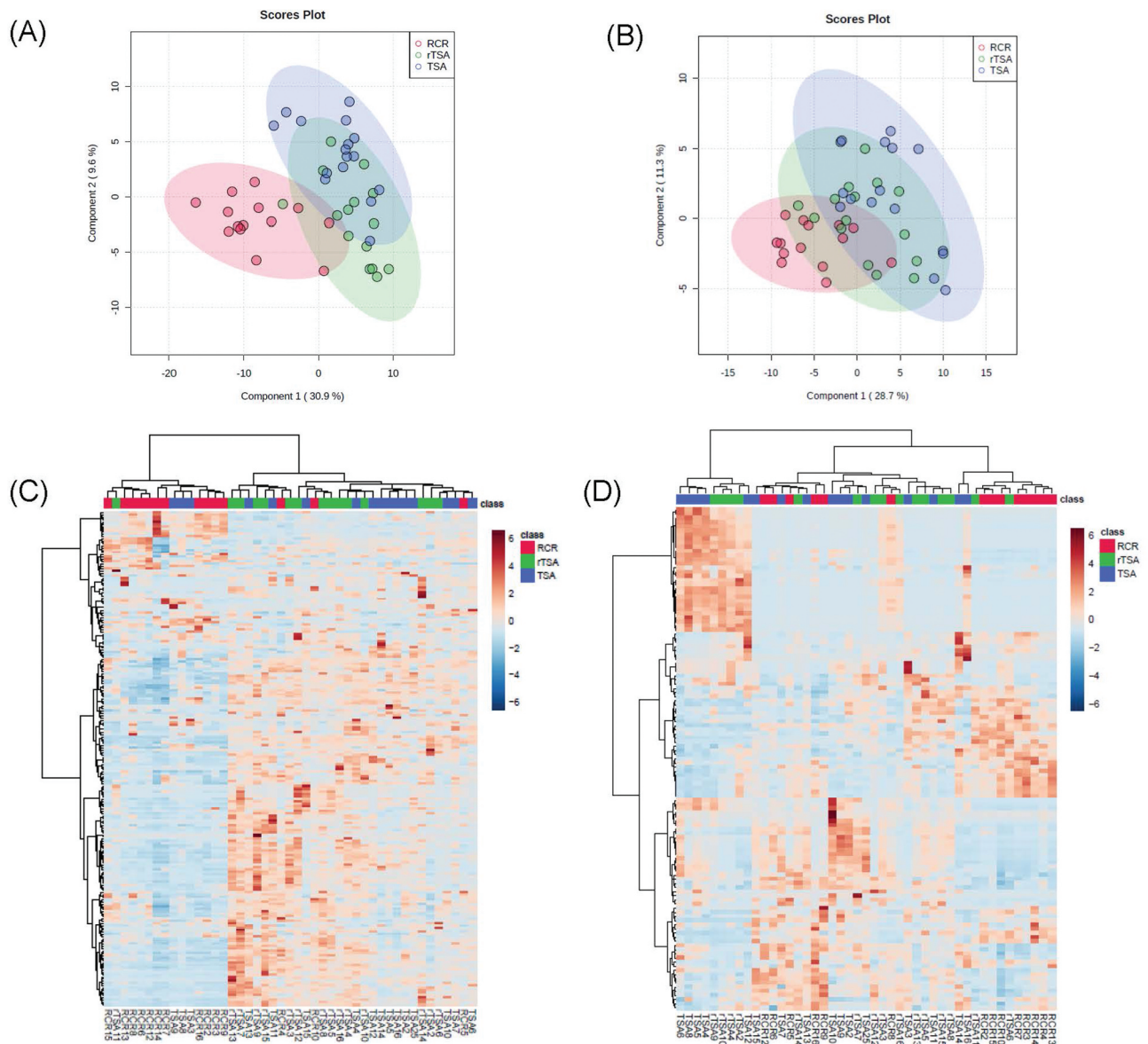


Figure 2. GCMS polar metabolite (A, C) and UPLCMS nonpolar metabolite (B, D) partial least-squares discriminant analysis (PLS-DA) Principal component plots (A-B) and heatmap clustering (C-D) for rotator cuff repair (RCR, acute tendon tear injury), reverse total shoulder arthroplasty (rTSA, chronic tendon degeneration), and total shoulder arthroplasty (TSA, tendon control) specimens.

intermediate metabolites.²⁷ As the central pathway, all identified metabolites in the TCA cycle including pyruvate ($p < 0.0001$; Figure 4(a)), citrate ($p = 0.01$, Figure 4(b)), isocitrate ($p = 0.008$, Figure 4(c)), 2-oxoglutarate ($p < 0.0001$, Figure 4(d)), Malate ($p = 0.001$; Figure 4(e)), and Fumarate ($p = 0.003$, Figure 4(f)), were decreased in RCR specimens relative to TSA controls. Metabolites in other pathways including alanine (beta- (3TMS), $p < 0.0001$), two asparagine derivatives (1: [-H₂O] (2TMS), $p = 0.003$; 2: (3TMS), $p = 0.01$), glutamate (glutamic acid (2TMS), $p = 0.002$), three glutamine derivatives (1: [-H₂O] (2TMS), $p = 0.04$, 2: [-H₂O] (3TMS), $p = 0.002$, 3: glutamine, DL (3TMS), $p = 0.005$), glycerate (glyceric acid (3TMS), $p = 0.03$),

lactate (lactic acid (2TMS), $p = 0.02$), and ornithine (4TMS, $p = 0.009$), were also decreased in RCR specimens relative to TSA controls (Supplemental 1). Notably, no sex-specific separation in metabolite abundance within each group was appreciated (Figure 4, open vs. closed symbols).

Reverse total shoulder arthroplasty (chronic injury) metabolomics

Relative to control TSA specimens, rTSA specimens taken at the time of surgery exhibited an overall increase in 14 polar GCMS metabolites (Figure 5(a)). Few nonpolar UPLCMS metabolites were significantly altered

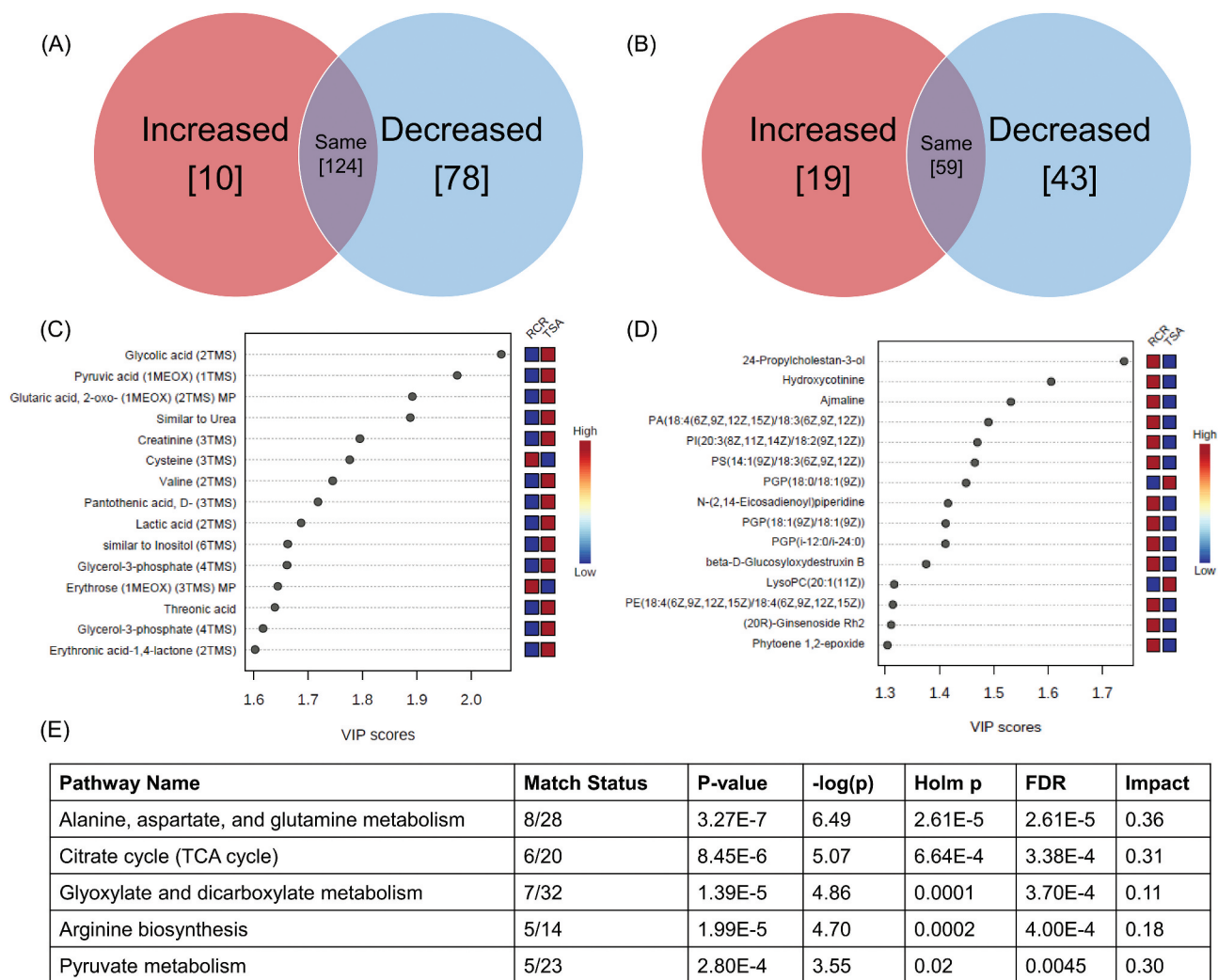


Figure 3. Metabolite comparisons between rotator cuff repair (RCR, acute tendon tear injury) and total shoulder arthroplasty (TSA, tendon control) specimens for GCMS nonpolar (A, C) and UPLCMS polar (B, D) metabolites demonstrating the number of significantly altered metabolites (A-B) and variable importance in projection (VIP) scores (C-D). Significant pathways (Holm p -value of < 0.05) from combined pathway analysis utilizing both polar and nonpolar significant metabolites (E).

(Figure 5(b)). VIP scoring demonstrated that Proline and an Amino Acid Derivative were the primary GCMS metabolites (Figure 5(c)), and a Phosphatidylserine, Triterpene Saponin (Tragopogonsaponin B), and Phosphatidylcholine were the primary UPLCMS metabolites driving metabolite profile separation (Figure 5(d)). When metabolites were individually analyzed, the nonspecific Amino Acid Derivative ($p = 0.0045$, Supplemental 1), Proline ($p = 0.006$, Figure 6(a)), and Phosphatidylserine ($p = 0.0092$, Supplemental 2) were found to be statistically increased in rTSA relative to TSA specimens. Tragopogonsaponin B ($p = 0.06$) and Phosphatidylcholine ($p = 0.07$) did not reach significance between groups (Supplemental 2).

Combined GCMS and UPLCMS pathway analysis revealed that a single pathway, Alanine, Aspartate, and Glutamate metabolism, demonstrated a Holm adjusted p -value of 0.02 denoting significance

(Figure 5(e)). While significant, the impact score of this pathway (which represents the importance of an individual pathway relative to the entire metabolic network) was 0.22 suggesting that metabolites in this pathway show changes but may not be fully driving biological changes within this pathway. Amino acids such as Alanine and Aspartate, which were significant metabolites in this pathway, and Lysine were all increased in rTSA specimens relative to TSA controls (Alanine $p = 0.001$, Figure 6(b); Aspartate $p = 0.01$, Figure 6(c); Lysine $p = 0.03$, Figure 6(d)). Notably, no sex-specific separation in metabolite abundance within each group was appreciated (Figure 6, open vs. closed symbols).

Given that rTSA specimens were portioned and utilized for both metabolomics and histology, a Spearman's correlative analysis was undertaken to

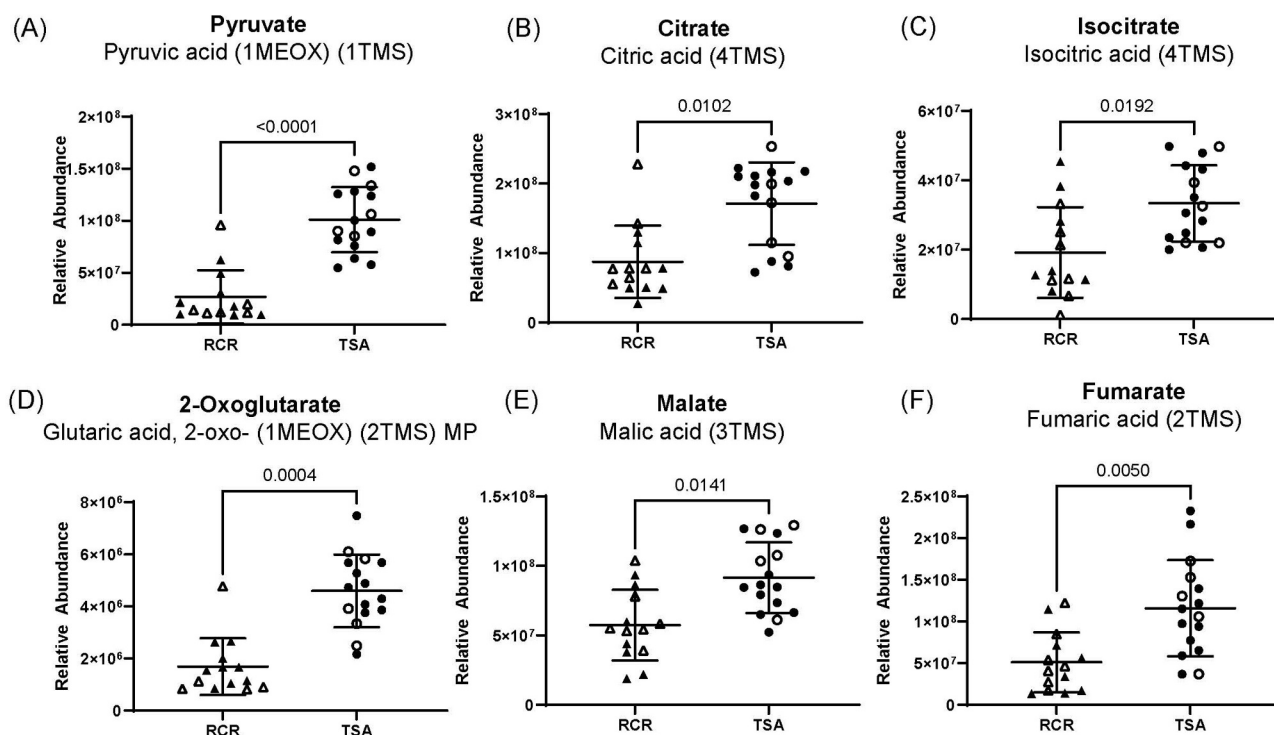


Figure 4. Significant alterations in citrate cycle (TCA cycle) inputs pyruvate (A) and intermediates citrate (B), isocitrate (C), 2-oxoglutarate (D), malate (E), and fumarate (F) in rotator cuff repair (RCR, acute tendon tear injury) specimens relative to total shoulder arthroplasty (TSA, tendon control) specimens. Data is presented as mean \pm STD with individual specimens denoted and p -values marked. Open symbols represent specimens from female patients and closed specimens represent specimens from male patients.

determine if metabolite levels were associated with varying degrees of tendon pathology. No significant correlations were observed following false-discovery rate corrections (Supplemental 7).

Discussion

The overarching goal of this study was to evaluate alterations to tendon metabolite profiles following acute tear or chronic degeneration of the rotator cuff. Relative to patients undergoing TSA (clinically unaffected tendon controls), tendons from patients undergoing RCR (acute tear injury) demonstrated distinct global metabolite profiles as compared to patients undergoing rTSA (chronic degeneration), as evidenced by PLS-DA analysis. Further classification of metabolite differences via individual metabolite comparisons and pathway analysis showed that acute injuries were associated with alterations to cellular pathways, while chronic injuries demonstrated alterations to pathways involved in extracellular matrix production and turnover. These specific pathways identified may assist in the development of novel treatment strategies to target both injury types.

Acute tears to the rotator cuff were associated with a shift toward decreased tendon metabolite abundance (121 of 333 polar and nonpolar metabolites; 36.3%). Altered metabolites were primarily associated with glycolic acid and decreased TCA cycle activity, both major players in cellular oxidative respiration and energetics. Increasingly in the last 10 years, poly-lactic-co-glycolic acid (PLGA), has been utilized in scaffolds and nanomaterials for the treatment of tendon injuries. PLGA scaffolds have been shown to have tunable mechanical properties,²⁸ suitable degradation and subsequent release kinetics of bioactive compounds,²⁹ and have performed favorably in preclinical tendon repair models.^{30–32} Further, exogenous glycolic acid moieties following polymer degradation may counteract decreased endogenous levels seen following injury; however, the specific role of PLGA or glycolic acid in tendon repair has yet to be determined.

The results herein also demonstrate that decreased TCA cycle activity is associated with acute tendon tear injuries. Conversely, transected rat Achilles tendons have shown increased TCA intermediates 1 week post-op,³³ and increased TCA activity *in-vitro* has been shown to stimulate human injured flexor tendon cells toward chondrogenic differentiation,³⁴ a known marker

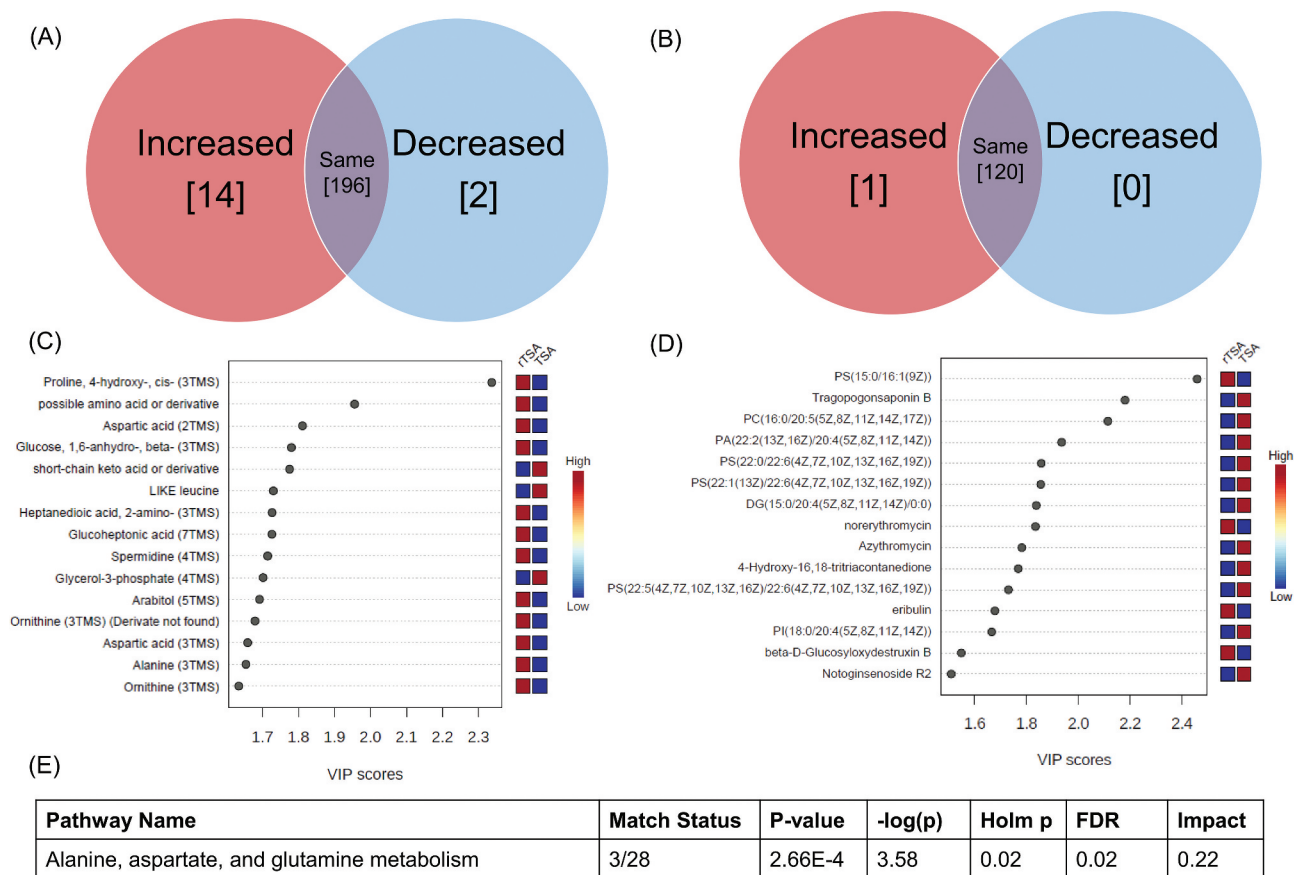


Figure 5. Metabolite comparisons between reverse total shoulder arthroplasty (rTSA, chronic tendon injury) and total shoulder arthroplasty (TSA, tendon control) specimens for GCMS nonpolar (A, C) and UPLCMS polar (B, D) metabolites demonstrating the number of significantly altered metabolites (A-B) and variable importance in projection (VIP) scores (C-D). Significant pathways (Holm p-value of < 0.05) from combined pathway analysis utilizing both polar and nonpolar significant metabolites (D).

of tendinopathy.^{35,36} As human tendons in the current study were collected between 1 and 48 months from injury diagnosis, a variable temporal response in TCA metabolite regulation may occur with injury, which should be further explored. Overall, the data supports that acute injury repair strategies should not only aim to provide structural continuity through bridging of tendon gaps but also maintain TCA cycle metabolism through additive bioactive compounds. Notably, the timing of TCA cycle maintenance should be considered as it relates to senescent, apoptotic, or necrotic tendon cellular mechanisms which have not been explored to date in relation to metabolic pathways.

Converse to acute tear injury, chronic degenerated tendon specimens from patients undergoing rTSA showed a shift toward increased metabolite abundance (15 of 333 polar and nonpolar metabolites; 4.5%). Specific metabolites identified as altered in the human specimens herein included phosphatidylserine, triterpene saponin (tragopogonsaponin b), phosphatidylcholine, and amino acids. Increased levels of

phosphatidylserine may be associated with apoptosis through targeted signaling of phagocytosis by macrophages, which has been previously shown to occur in Achilles tendon cells.³⁷ To date, no relationship could be identified between tendon and triterpene saponin (tragopogonsaponin b), as this metabolite is primarily associated with plants and may be nonspecific. We have previously shown using a mouse model of chronic tendinopathy that initiating injury was associated with increased metabolic activity using both transcriptomic³⁸ and metabolomic³⁹ methods, particularly during the early phase of tendon degeneration. Specifically, increased phosphatidylcholine metabolites were evident,³⁹ so it is interesting that injured human tendon specimens herein conversely showed decreased levels relative to controls. Notably, phosphatidylcholine has been associated with enhanced lubrication during tendon injuries⁴⁰ and may be important in myotendinous maintenance,^{41,42} which is particularly relevant for the rotator cuff. As chronic specimens were collected over a large timeframe (time from

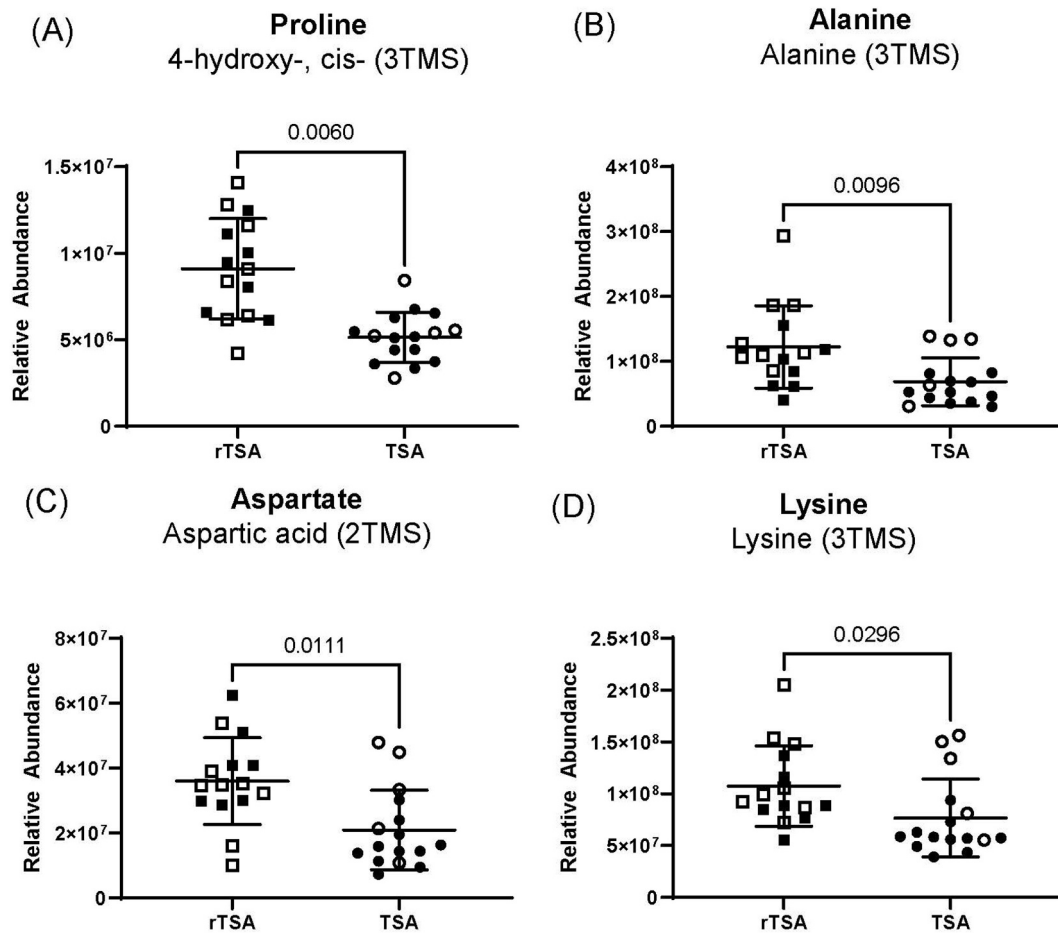


Figure 6. Significant alterations in amino acids including proline (A), alanine (B) and aspartate (C), and lysine (D) in reverse total shoulder arthroplasty (rTSA, chronic tendon injury) specimens relative to total shoulder arthroplasty (TSA, tendon control) specimens. Data is presented as mean \pm STD with individual specimens denoted and p-values marked. Open symbols represent specimens from female patients and closed specimens represent specimens from male patients.

diagnosis 1.5–7.0 months), differences in phosphatidylcholine changes between mouse and human specimens may indicate a temporal chronic injury response. Therefore, future preclinical studies should control for the level of chronicity (early, moderate, end-stage).

Most notably, chronic injury was associated with increased levels of the amino acids' alanine, aspartate, lysine, and proline. A systemic review recently touted the importance of amino acid synthesis on tendon and muscle healing,⁴³ however controlled studies are needed to fully understand the ramifications before use in clinical practice. Generally, the role of individual amino acids has been understudied in tendon. Amino acid racemization (enantiomer conversion), specifically with aspartate, has been used as a measure of collagen turnover in tendon.⁴⁴ Collagen is comprised of a repeating triplet of X-Y-Glycine residues with X primarily being proline (28%) and Y primarily hydroxyproline (38%).⁴⁵ The other proportions of

X and Y can be any other amino acid; therefore, any change in the amino acid metabolite pool, may have ramifications on collagen synthesis, turnover, and organization, which have all been implicated to play a role in tendinopathy.⁴⁶ In humans, the alanine, aspartate, lysine, and proline amino acid composition of the alpha-1 chains of collagen type I (COL1), collagen type II (COL2), and collagen type III (COL3) are very similar, with maximum variations of 1.7% seen between these three collagen types.⁴⁷ As these are the most commonly studied collagen variants associated with injury, further research is needed to understand how relatively small variations in amino acid composition may affect fibrotic scar tissue formation (higher abundance of COL3 to COL1) in acute injury¹³ and chondroid metaplasia (increased COL2 abundance) in chronic injury.^{6,7,9}

Indeed, scurvy, osteogenesis imperfecta, and Ehlers Danlos syndrome directly affect the collagen amino acid structure, inhibiting proper organization,

stabilization, and/or function. In osteogenesis imperfecta, the majority of cases are caused by another amino acid replacing every third glycine.⁴⁸ Scurvy is associated with decreased ascorbic acid which results in inhibition of proline and lysine hydroxylation for appropriate collagen organization.⁴⁹ Types of Ehlers Danlos syndrome result from deficiency in lysyl-hydroxylase inhibiting the hydroxylation of lysine residues for appropriate cross-linking of collagen trimers.⁵⁰ Further work is needed to delineate the specific role of individual amino acids in degenerative tendon disease for the identification of potential treatment interventions. Of note, disproportionate patient sex demographics may have contributed to differences between rTSA (chronic degenerated) and TSA (clinically unaffected tendon control) specimens. While there were a higher proportion of female rTSA specimens and male TSA specimens, sex-specific separation in metabolite abundance was not evident when individual metabolites were analyzed in this study. Future work will seek to delineate the role that sex may play in tendon metabolism.

Limitations of the current study include the size of specimens obtained from patients undergoing RCR and TSA. Due to the small size, these specimens could not be utilized for both metabolomics and histology, which was possible for the rTSA specimens. Therefore, metabolite levels could not be directly correlated to pathologic features. Additionally, rTSA patients were significantly older than both RCR and TSA (histology) patients. Therefore, the histological pathology differences between rTSA and TSA specimens may be associated with age-related effects. Interestingly, TSA specimens showed some mild, age-related degenerative changes on histopathology. Therefore, despite the age differences, tissue-related aging changes may have been accounted for in the experimental design. Importantly, no difference in age between rTSA and TSA (metabolomics) specimens was evident. As RCR and rTSA metabolite profiles were not directly compared, the difference in age has little effect on the current study, except when considering global metabolite differences between those groups. As no studies to date have sought to determine age-related effects of metabolism on tendon, the influence of this factor is unknown.

In summary, this study demonstrates that metabolite profiles are associated with injury type and reiterates that acute tears and chronic degeneration of the rotator cuff tendons should be treated distinctly. While we primarily consider acute tear injuries to be associated with a loss or extracellular matrix continuity, we found that cellular metabolic pathways were altered with injury type. Conversely, while we typically consider

chronic injury to be associated with degenerative cellular and subsequent nuanced extracellular matrix changes, we found that metabolic pathways associated with extracellular production and turnover were primarily altered. Therefore, therapeutic strategies should address both cellular and matrix changes regardless of the type of injury induction. Overall, the specific pathways identified, paired with validated, established methods (scaffolds, physical rehabilitation), may serve as novel therapeutic targets for patients who suffer from both acute tears and chronic degeneration of the rotator cuff tendons.

Acknowledgments

The authors would like to acknowledge Colorado State University researchers Linxing Yao, PhD, and Corey Broeckling, PhD of the Analytical Resources Core - Bioanalysis and Omics (ARC-BIO) for their assistance in the metabolomics work, and Ann Hess, PhD of the Graybill Statistics Laboratory for her assistance with the statistical analyses.

Disclosure statement

No potential conflict of interest was reported by the author(s).

Funding

Funding for this project was aided by a grant from the Orthopaedic Research and Education Foundation (KJS).

Author contribution statements

All authors have read and approved the final manuscript:
 KJS: Experimental Design, Metabolomics Specimen Preparation, Data Analysis, Statistics, Manuscript Preparation
 KA: Histopathology, Manuscript Review
 SW: Histology, Manuscript Review
 NV: Specimen Retrieval, Manuscript Review
 AY: Specimen Retrieval, Manuscript Review
 KSS: Histopathology, Histopathology Interpretation, Manuscript Review
 DDF: Clinical Interpretation, Manuscript Review
 BJC: Specimen Retrieval, Clinical Interpretation, Manuscript Review

ORCID

Katie J. Sikes  <http://orcid.org/0000-0002-3750-4777>
 Adam B. Yanke  <http://orcid.org/0000-0002-9601-4217>
 Kelly S. Santangelo  <http://orcid.org/0000-0002-2348-594X>
 Brian J. Cole  <http://orcid.org/0000-0002-4006-2113>

References

- Longo UG, Franceschi F, Ruzzini L, Spiezia F, Maffulli N, Denaro V. Higher fasting plasma glucose levels within the normoglycaemic range and rotator cuff tears. *Br J Sports Med.* 2009;43(4):284–287. doi:10.1136/bjism.2008.049320.
- Rechardt M, Shiri R, Karppinen J, Jula A, Heliövaara M, Viikari-Juntura E. Lifestyle and metabolic factors in relation to shoulder pain and rotator cuff tendinitis: a population-based study. *BMC Musculoskelet Disord.* 2010;11(1):165. doi:10.1186/1471-2474-11-165.
- Ranger TA, Wong AM, Cook JL, Gaida JE. Is there an association between tendinopathy and diabetes mellitus? A systematic review with meta-analysis. *Br J Sports Med.* 2016;50(16):982–989. doi:10.1136/bjsports-2015-094735.
- Soslowky LJ, Fryhofer GW. Tendon homeostasis in hypercholesterolemia. *Adv Exp Med Biol.* 2016;920:151–165.
- Andia I, Abate M. Hyperuricemia in Tendons. *Adv Exp Med Biol.* 2016;920:123–132.
- Huegel J, Williams AA, Soslowky LJ. Rotator cuff biology and biomechanics: a review of normal and pathological conditions. *Curr Rheumatol Rep.* 2015;17(1):476. doi:10.1007/s11926-014-0476-x.
- Jarvinen M, Jozsa L, Kannus P, Jarvinen TL, Kvist M, Leadbetter W. Histopathological findings in chronic tendon disorders. *Scand J Med Sci Sports.* 1997;7(2):86–95. doi:10.1111/j.1600-0838.1997.tb00124.x.
- Kannus P, Jozsa L. Histopathological changes preceding spontaneous rupture of a tendon. A controlled study of 891 patients. *J Bone Joint Surg Am.* 1991;73(10):1507–1525. doi:10.2106/00004623-199173100-00009.
- Khan KM, Cook JL, Bonar F, Harcourt P, Astrom M. Histopathology of common tendinopathies. Update and implications for clinical management. *Sports Med.* 1999;27(6):393–408. doi:10.2165/00007256-199927060-00004.
- Pingel J, Lu Y, Starborg T, Fredberg U, Langberg H, Nedergaard A, Weis M, Eyre D, Kjaer M, Kadler KE. 3-D ultrastructure and collagen composition of healthy and overloaded human tendon: evidence of tenocyte and matrix buckling. *J Anat.* 2014;224(5):548–555. doi:10.1111/joa.12164.
- Jozsa L, Balint BJ, Reffy A, Demel Z. Fine structural alterations of collagen fibers in degenerative tendinopathy. *Arch Orthop Trauma Surg* (1978). 1984;103(1):47–51. doi:10.1007/BF00451318.
- Tashjian RZ. Epidemiology, natural history, and indications for treatment of rotator cuff tears. *Clin sports med.* *Clin Sports Med.* 2012;31(4):589–604. doi:10.1016/j.csm.2012.07.001.
- Jarvinen TA, Kannus P, Maffulli N, Khan KM. Achilles tendon disorders: etiology and epidemiology. *foot Ankle Clin.* *Foot Ankle Clinics.* 2005;10(2):255–266. doi:10.1016/j.fcl.2005.01.013.
- Ackerman JE, Best KT, Muscat SN, Loisel AE. Metabolic regulation of tendon inflammation and healing following injury. *Curr Rheumatol Rep.* 2021;23(3):15. doi:10.1007/s11926-021-00981-4.
- Lee HJ, Hong OK, Kwak DH, Kim YS. Metabolic profiling of serum and tissue from the rotator interval and anterior capsule in shoulder stiffness: a preliminary study. *BMC Musculoskelet Disord.* 2019;20(1):364. doi:10.1186/s12891-019-2709-7.
- Shinozaki T, Takagishi K, Ichikawa A, Inoue T, Yamaji T, Ishikawa T, Ohsawa T, Aramaki M, Aiba S, Endo K. Use of 2-[18F]-fluoro-2-deoxy-d-glucose positron emission tomography (FDG PET) imaging for the evaluation of muscle metabolic activity in ruptured rotator cuffs: identification of shoulder muscles by fusion imaging studies involving both FDG PET and magnetic resonance imaging. *J Shoulder Elb Surg.* 2003;12(6):544–549. doi:10.1016/s1058-2746(03)00208-8.
- Shinozaki T, Takagishi K, Ohsawa T, Yamaji T, Endo K. Pre- and postoperative evaluation of the metabolic activity in muscles associated with ruptured rotator cuffs by 18 F-FDG PET imaging. *Clin Physiol Funct Imag.* 2006;26(6):338–342. doi:10.1111/j.1475-097X.2006.00698.x.
- Chatterjee M, Evans MK, Bell R, Nguyen PK, Kamalidinov TB, Korntner S, Kuo CK, Dymont NA, Andarawis-Puri N. Histological and immunohistochemical guide to tendon tissue. *J Orthop Res.* 2023;41(10):2114–2132. doi:10.1002/jor.25645.
- Cook JL, Feller JA, Bonar SF, Khan KM. Abnormal tenocyte morphology is more prevalent than collagen disruption in asymptomatic athletes' patellar tendons. *J Orthop Res.* 2004;22(2):334–338. doi:10.1016/j.orthres.2003.08.005.
- Movin T, Gad A, Reinholt FP, Rolf C. Tendon pathology in long-standing achillodynia. Biopsy findings in 40 patients. *Acta Orthop Scand.* 1997;68(2):170–175. doi:10.3109/17453679709004002.
- Broeckling CD, Afsar FA, Neumann S, Ben-Hur A, Prenni JE. Ramclust: a novel feature clustering method enables spectral-matching-based annotation for metabolomics data. *Anal Chem.* 2014;86(14):6812–6817. doi:10.1021/ac501530d.
- Broeckling CD, Heuberger AL, Prince JA, Ingelsson E, Prenni JE. Assigning precursor-product ion relationships in indiscriminant MS/MS data from non-targeted metabolite profiling studies. *Metabolomics.* 2012;9(1):33–43. doi:10.1007/s11306-012-0426-4.
- Jaeger C, Meret M, Schmitt CA, Lisec J. Compound annotation in liquid chromatography/high-resolution mass spectrometry based metabolomics: robust adduct ion determination as a prerequisite to structure prediction in electrospray ionization mass spectra. *Rapid Commun Mass Spectrom.* 2017;31(15):1261–1266. doi:10.1002/rcm.7905.
- Djombou Feunang Y, Eisner R, Knox C, Chepelev L, Hastings J, Owen G, Fahy E, Steinbeck C, Subramanian S, Bolton E, et al. ClassyFire: automated chemical classification with a comprehensive, computable taxonomy. *J Cheminform.* 2016;8(1):61. doi:10.1186/s13321-016-0174-y.
- Kopka J, Schauer N, Krueger S, Birkemeyer C, Usadel B, Bergmüller E, Dormann P, Weckwerth W, Gibon Y, Stitt M, et al. GMD@CSB.DB: the golm

- metabolome database. *Bioinformatics*. 2005;21(8):1635–1638. doi:10.1093/bioinformatics/bti236.
26. Chong J, Xia J. Using MetaboAnalyst 4.0 for metabolomics data analysis, interpretation, and integration with other omics data. *Methods Mol Biol*. 2020;2104:337–360.
 27. Arnold PK, Finley LWS. Regulation and function of the mammalian tricarboxylic acid cycle. *J Biol Chem*. 2023;299(2):102838. doi:10.1016/j.jbc.2022.102838.
 28. Kumber SG, Nukavarapu SP, James R, Nair LS, Laurencin CT. Electrospun poly(lactic acid-co-glycolic acid) scaffolds for skin tissue engineering. *Biomaterials*. 2008;29(30):4100–4107. doi:10.1016/j.biomaterials.2008.06.028.
 29. Shi X, Zhao Y, Zhou J, Chen S, Wu H. One-step generation of engineered drug-laden poly(lactic-co-glycolic acid) micropatterned with Teflon chips for potential application in tendon restoration. *ACS Appl Mater Interface*. 2013;5(21):10583–10590. doi:10.1021/am402388k.
 30. Yu YH, Shen SJ, Hsu YH, Chou YC, Yu PC, Liu SJ. Tri-layered doxycycline-, collagen- and bupivacaine-loaded Poly(lactic-co-glycolic acid) nanofibrous scaffolds for tendon rupture repair. *Polym (Basel)*. 2022;14(13):14(13). doi:10.3390/polym14132659.
 31. Vaquette C, Slimani S, Kahn CJ, Tran N, Rahouadj R, Wang X. A poly(lactic-co-glycolic acid) knitted scaffold for tendon tissue engineering: an in vitro and in vivo study. *J Biomater Sci Polym Ed*. 2010;21(13):1737–1760. doi:10.1163/092050609X12560455246676.
 32. Chen P, Cui L, Fu SC, Shen L, Zhang W, You T, Ong TY, Liu Y, Yung SH, Jiang C. The 3D-Printed PLGA scaffolds loaded with bone marrow-derived mesenchymal stem cells augment the healing of rotator cuff repair in the rabbits. *Cell Transpl*. 2020;29:963689720973647. doi:10.1177/0963689720973647.
 33. Zhang K, Hast MW, Izumi S, Usami Y, Shetye S, Akabudike N, Philp NJ, Iwamoto M, Nissim I, Soslowsky LJ, et al. Modulating glucose metabolism and lactate synthesis in injured mouse tendons: treatment with dichloroacetate, a lactate synthesis inhibitor, improves tendon healing. *Am J Sports Med*. 2018;46(9):2222–2231. doi:10.1177/0363546518778789.
 34. Izumi S, Otsuru S, Adachi N, Akabudike N, Enomoto-Iwamoto M, Dong Y. Control of glucose metabolism is important in tenogenic differentiation of progenitors derived from human injured tendons. *PLoS One*. 2019;14(3):e0213912. doi:10.1371/journal.pone.0213912.
 35. Parkinson J, Samiric T, Ilic MZ, Cook J, Feller JA, Handley CJ. Change in proteoglycan metabolism is a characteristic of human patellar tendinopathy. *Arthritis Rheum*. 2010;62(10):3028–3035. doi:10.1002/art.27587.
 36. Parkinson J, Samiric T, Ilic MZ, Cook J, Handley CJ. Involvement of proteoglycans in tendinopathy. *J Musculoskelet Neuronal Interact*. 2011;11(2):86–93.
 37. Scott A, Khan KM, Duronio V. IGF-I activates PKB and prevents anoxic apoptosis in achilles tendon cells. *J Orthop Res*. 2005;23(5):1219–1225. doi:10.1016/j.orthres.2004.12.011.
 38. Sikes KJ, Li J, Gao SG, Shen Q, Sandy JD, Plaas A, Wang VM. Tgf-b1 or hypoxia enhance glucose metabolism and lactate production via HIF1A signaling in tendon cells. *Connect Tissue Res*. 2018;59(5):458–471. doi:10.1080/03008207.2018.1439483.
 39. Sikes KJ, McConnell A, Serkova N, Cole B, Frisbie D. Untargeted metabolomics analysis identifies creatine, myo-inositol, and lipid pathway modulation in a murine model of tendinopathy. *J Orthop Res*. 2022;40(4):965–976. doi:10.1002/jor.25112.
 40. Moro-Oka T, Miura H, Mawatari T, Kawano T, Nakanishi Y, Higaki H, Iwamoto Y. Mixture of hyaluronic acid and phospholipid prevents adhesion formation on the injured flexor tendon in rabbits. *J Orthop Res*. 2000;18(5):835–840. doi:10.1002/jor.1100180523.
 41. Patriarca P, Zatti M, Gompertz D. Fatty acid composition of the phosphatidylcholine fractions of denervated and tendonectomized rat skeletal muscle. *Biochem J*. 1969;115(5):1079–1080. doi:10.1042/bj1151079.
 42. Heiner L, Domonkos J, Vargha M. Effect of tenotomy on the lipid composition of muscles with different biological functions. *Acta Physiol Acad Sci Hung*. 1974;45(3–4):163–171.
 43. Tack C, Shorthouse F, Kass L. The physiological mechanisms of effect of vitamins and amino acids on tendon and muscle healing: a systematic review. *Int J Sport Nutr Exerc Metab*. 2018;28(3):294–311. doi:10.1123/ijsnem.2017-0267.
 44. Thorpe CT, Streeter I, Pinchbeck GL, Goodship AE, Clegg PD, Birch HL. Aspartic acid racemization and collagen degradation markers reveal an accumulation of damage in tendon collagen that is enhanced with aging. *J Biol Chem*. 2010;285(21):15674–15681. doi:10.1074/jbc.M109.077503.
 45. Shoulders MD, Raines RT. Collagen structure and stability. *Annu Rev Biochem*. 2009;78(1):929–958. doi:10.1146/annurev.biochem.77.032207.120833.
 46. Samiric T, Parkinson J, Ilic MZ, Cook J, Feller JA, Handley CJ. Changes in the composition of the extracellular matrix in patellar tendinopathy. *Matrix Biol*. 2009;28(4):230–236. doi:10.1016/j.matbio.2009.04.001.
 47. Nassa M, Anand P, Jain A, Chhabra A, Jaiswal A, Malhotra U, Rani V. Analysis of human collagen sequences. *Bioinformation*. 2012;8(1):26–33. doi:10.6026/97320630008026.
 48. Kuivaniemi H, Tromp G, Prockop DJ. Mutations in collagen genes: causes of rare and some common diseases in humans. *FASEB J*. 1991;5(7):2052–2060. doi:10.1096/fasebj.5.7.2010058.
 49. Rebouche CJ. Ascorbic acid and carnitine biosynthesis. *Am J Clin Nutr*. 1991;54(6 Suppl):1147S–1152S. doi:10.1093/ajcn/54.6.1147s.
 50. Mao JR, Bristow J. The Ehlers-Danlos syndrome: on beyond collagens. *J Clin Invest*. 2001;107(9):1063–1069. doi:10.1172/JCI12881.